

See discussions, stats, and author profiles for this publication at: <https://www.researchgate.net/publication/275339530>

# Elusive Presence of Chloride in Mixed Halide Perovskite Solar Cells

ARTICLE *in* JOURNAL OF PHYSICAL CHEMISTRY LETTERS · SEPTEMBER 2014

Impact Factor: 7.46

---

READS

138

1 AUTHOR:



Sofia Masi

Università del Salento

6 PUBLICATIONS 41 CITATIONS

[SEE PROFILE](#)

## Elusive Presence of Chloride in Mixed Halide Perovskite Solar Cells

Silvia Colella,<sup>\*,†</sup> Edoardo Mosconi,<sup>‡</sup> Giovanna Pellegrino,<sup>\*,§</sup> Alessandra Alberti,<sup>§</sup>  
Valentino L. P. Guerra,<sup>†,▽</sup> Sofia Masi,<sup>†,‡,▽</sup> Andrea Listorti,<sup>†,‡</sup> Aurora Rizzo,<sup>†</sup>  
Guglielmo Guido Condorelli,<sup>#</sup> Filippo De Angelis,<sup>\*,‡</sup> and Giuseppe Gigli<sup>†,‡,▽</sup>

<sup>†</sup>NNL – National Nanotechnology Laboratory, CNR Istituto Nanoscienze, Distretto Tecnologico, Via Arnesano 16, 73100 Lecce, Italy

<sup>‡</sup>Computational Laboratory for Hybrid/Organic Photovoltaics (CLHYO), CNR-ISTM, Via Elce di Sotto 8, Perugia I-06123, Italy

<sup>§</sup>CNR-IMM, Istituto per la Microelettronica e Microsistemi, Strada VIII n°S, 95121 Catania, Italy

<sup>‡</sup>Center for Bio-Molecular Nanotechnology, Fondazione Istituto Italiano di Tecnologia, Via Barsanti, 73010 Arnesano (Lecce), Italy

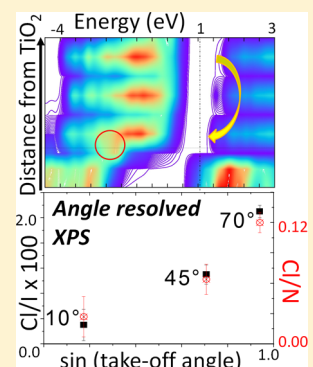
<sup>#</sup>Università degli studi di Catania and INSTM UdR Catania, Viale Andrea Doria 6, 95125 Catania, Italy

<sup>▽</sup>Dipartimento di Matematica e Fisica “E. De Giorgi”, Università del Salento, Via per Arnesano, 73100 Lecce, Italy

### Supporting Information

**ABSTRACT:** The role of chloride in the  $\text{MAPbI}_{3-x}\text{Cl}_x$  perovskite is still limitedly understood, albeit subjected of much debate. Here, we present a combined angle-resolved X-ray photoelectron spectroscopy (AR-XPS) and first-principles DFT modeling to investigate the  $\text{MAPbI}_{3-x}\text{Cl}_x/\text{TiO}_2$  interface. AR-XPS analyses carried out on ad hoc designed bilayers of  $\text{MAPbI}_{3-x}\text{Cl}_x$  perovskite deposited onto a flat  $\text{TiO}_2$  substrate reveal that the chloride is preferentially located in close proximity to the perovskite/ $\text{TiO}_2$  interface. DFT calculations indicate the preferential location of chloride at the  $\text{TiO}_2$  interface compared to the bulk perovskite due to an increased chloride– $\text{TiO}_2$  surface affinity. Furthermore, our calculations clearly demonstrate an interfacial chloride-induced band bending, creating a directional “electron funnel” that may improve the charge collection efficiency of the device and possibly affecting also recombination pathways. Our findings represent a step forward to the rationalization of the peculiar properties of mixed halide perovskite, allowing one to further address material and device design issues.

**SECTION:** Energy Conversion and Storage; Energy and Charge Transport



The field of solid-state solution-processable photovoltaics has experienced in the recent years a deep transformation thanks to the exploitation of the emergent class of self-assembling lead halide hybrid perovskites. Their revolutionary role in pushing the solar conversion efficiency up to 19.3%<sup>1</sup> has to be ascribed to the unique combination of advantages that they present, including the intense and extended light harvesting and the superior, ambipolar charge-transport properties.<sup>2</sup> Their crystalline structure allows an easy interchange of the components, enabling a fine-tuning of the material properties. For these characteristics, solar cells have been assembled in a variety of architectures, either in mesostructures or planar thin film devices, involving different preparation routes and possible morphology of the final compounds.<sup>3–6</sup>

The most widely studied and performing materials, the leading players in this evolution, are methylammonium tri-iodide lead perovskite ( $\text{MAPbI}_3$ ) and its mixed iodide–chloride analogue ( $\text{MAPbI}_{3-x}\text{Cl}_x$ ). The two materials possess the same basic crystalline structure and optical band gap; however, they significantly differ when embedded in solar converting devices, and this has been ascribed to the superior exciton/free charges diffusion length and reduced recombination of MAP-

$\text{bI}_{3-x}\text{Cl}_x$ .<sup>7–9</sup> As a proof of the unique concomitant capability of both absorbing light and transporting charges to the collecting electrode, the  $\text{MAPbI}_{3-x}\text{Cl}_x$  mixed halide perovskite has been for the first time employed on an inert  $\text{Al}_2\text{O}_3$  scaffold, replacing the standard mesoporous  $\text{TiO}_2$  electrode commonly employed in dye-sensitized solar cells (DSSCs).<sup>9</sup> Most notably, the two materials significantly differ in their charge recombination behavior, with  $\text{MAPbI}_{3-x}\text{Cl}_x$  showing distinctively lower recombination rates compared to  $\text{MAPbI}_3$ .<sup>7–9</sup> The decisive function of chloride has been recently demonstrated by tuning the MACl percentage in the mixed halide perovskite and directly verifying its influence on the film morphology/formation and on the material optoelectronic properties.<sup>10,11</sup> However, unexpectedly, it has been reported that the vast majority of the chloride ions present in the precursor solution are not detectable in the final material, within the technique detection limit, by either “bulk” analytic techniques, such as energy dispersive X-ray spectroscopy (EDX) and electron

**Received:** September 3, 2014

**Accepted:** September 29, 2014

**Published:** September 29, 2014

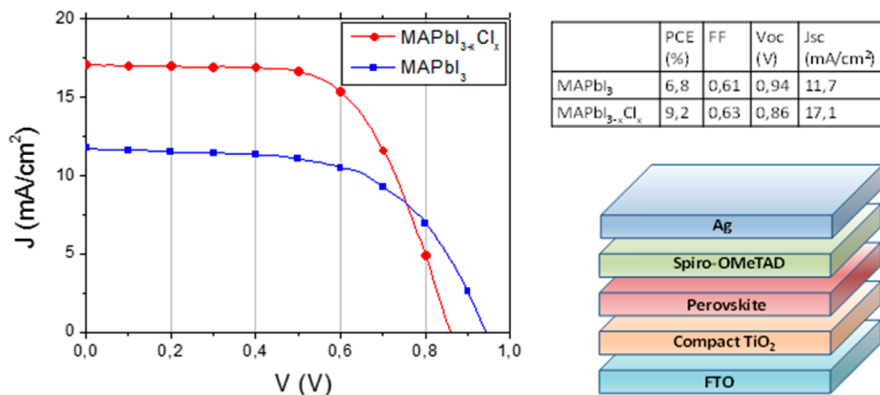


**Figure 1.** (a)  $I$ – $V$  curves under illumination of the best-performing devices. (b) Table summarizing the photovoltaic parameters and sketch of the planar heterojunction device structure.

energy loss spectroscopy (EELS), or by surface-sensitive X-ray photoelectron spectroscopy (XPS) measurements.<sup>10–12</sup>

Thus, understanding the specific effect that chloride doping plays in affecting and somehow determining the properties of mixed halide perovskites and/or its presence and location in perovskite films remains one of the most discussed open questions within the scientific community. In particular, a survey of the literature clearly suggests very little chloride incorporation into the perovskite film.<sup>9,13–15</sup> Aiming at rationalizing the effect of chloride doping in MAPbI<sub>3-x</sub>Cl<sub>x</sub>, we focus here on revealing the possible location of chloride in typical device assemblies, such as that shown in Figure 1 (FTO/compact TiO<sub>2</sub>/MAPbI<sub>3-x</sub>Cl<sub>x</sub>/spiro-OMeTAD/Ag).<sup>16–19</sup> To this aim, we implemented a simplified device architecture with the MAPbI<sub>3-x</sub>Cl<sub>x</sub> active component scaled down to a few nanometers. We used such a system to investigate through a nondestructive approach, namely, angle-resolved X-ray photoelectron spectroscopy (AR-XPS), the elemental composition along the perovskite thickness and to assess the chloride distribution within the MAPbI<sub>3-x</sub>Cl<sub>x</sub> layer.

The interface of interest, namely, a planar MAPbI<sub>3-x</sub>Cl<sub>x</sub>/TiO<sub>2</sub> heterojunction, has been tested in solar cells in comparison with the device based on MAPbI<sub>3</sub> using the device architecture sketched in Figure 1. Figure 1 also reports the  $I$ – $V$  curves of the best-performing devices within the two series, obtained by employing comparable deposition conditions for the two materials. We have verified that such device geometry leads to an efficiency of 9.2% for MAPbI<sub>3-x</sub>Cl<sub>x</sub> in line with the values reported in the literature<sup>6,20–22</sup> for the same architecture and deposition technique. The neat MAPbI<sub>3</sub> device presents significantly lower performances compared to the state of the art<sup>23</sup> due to the nonoptimal concentration of the precursor solution that we purposely employed here to realize a valuable comparison with the Cl-based counterpart. Notably, both the open-circuit voltage ( $V_{oc}$ ) and fill factor (FF) are in accordance with the literature scenario,<sup>23–25</sup> confirming the quality of the devices and allowing for a valid comparison between pure and mixed perovskite solar cells.

The absorption spectra of the two films (see Figure S1, Supporting Information) reveal higher light-harvesting capability for MAPbI<sub>3-x</sub>Cl<sub>x</sub> that partially explains the higher photocurrent extracted in the device, also attributable to the charge collection efficiency through the mixed perovskite improved by the presence of chloride, as previously demonstrated.<sup>26</sup>

Other factors being essentially similar for the two perovskites, we have hypothesized that chloride could possibly be located on the TiO<sub>2</sub> surface, as theoretically suggested,<sup>27</sup> thus possibly influencing the energetics and electronic structure of the perovskite/TiO<sub>2</sub> interface.

To test this hypothesis, we performed AR-XPS measurements on ~5 nm thin MAPbI<sub>3-x</sub>Cl<sub>x</sub> perovskite layers deposited onto flat TiO<sub>2</sub> substrates.<sup>16–19</sup> The flat TiO<sub>2</sub> layer was deposited by a sputtering technique to have a precise control over the thickness, roughness, and uniformity. Thin perovskite layers deposited onto the flat TiO<sub>2</sub> substrates were prepared by using a very diluted MAPbI<sub>3-x</sub>Cl<sub>x</sub> solution (1.5 wt % in dimethylformamide (DMF) solution). X-ray diffraction (XRD) analyses were performed on the discussed sample, showing the characteristic, even though low intensity, peak at  $2\theta = 14.1^\circ$  attributed to the perovskite structure (Figure S2, Supporting Information). More defined XRD patterns of slightly thicker films (Figure S3, Supporting Information), obtained from more concentrated solutions (3 wt %), gave a further confirmation of the perovskite formation. The thickness of the perovskite film was evaluated by X-ray reflectivity (Figure S4, Supporting Information) to be extremely thin ( $5 \pm 4$  nm). The coverage is characterized by grains uniformly covering the TiO<sub>2</sub> surface, as evidenced by atomic force microscopy inspection (Figure S5, Supporting Information).

The XPS spectra have been collected on such a prepared sample at three different photoelectron (p.e.) takeoff angles with respect to the sample surface, that is, 10, 45, and 70°, with the purpose of progressively exploring the layer depth. All of the acquisitions show the presence of spectral contributions from perovskite elements (lead, nitrogen, chlorine, and iodine) and those from the underneath substrate (titanium and oxygen) (Figure S6, Supporting Information). Notably, the intensities of the Ti 2p and the O 1s contributions exponentially decrease by progressively reducing the p.e. takeoff angle, in keeping with the formation of a uniform perovskite layer. A certain amount of adventitious carbon physisorbed on the sample surface is also detected in all of the spectra with a percentage that, consistently, diminishes by increasing the p.e. takeoff angle. The C 1s contribution was thus used to calibrate the binding energy (BE) scale.

In Figure 2, the XPS spectra collected in the Cl 2p region at the three different p.e. takeoff angles are shown. In all of the cases, the Cl 2p<sub>3/2</sub> spin-orbit component is centered at 198.4 eV, compatible with the presence of Cl atoms in the form of chloride.<sup>28</sup> As clearly visible from Figure 2, the intensity of the

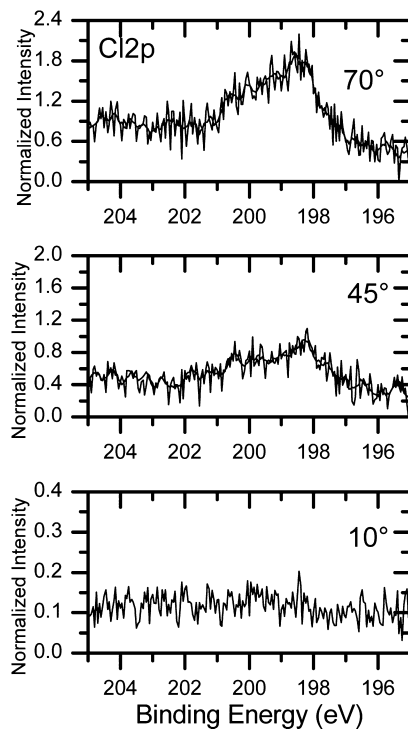


**Figure 2.** XPS Cl 2p region as revealed at p.e. takeoff angles of 70, 45, and 10° in the  $\text{MAPbI}_{3-x}\text{Cl}_x/\text{TiO}_2$  bilayer.

Cl signal progressively varies with the p.e. takeoff angle of the photoelectrons and, thus, with the sampling depth. In particular, the intensity of the Cl 2p signal is considerably suppressed to a value below the detection limit at the lowest takeoff angle (10°), while it is clearly enhanced (beyond the measurement accuracy) at the highest takeoff angle (70°). In order to compare the depth distribution of Cl with those of other elements in the perovskite, the relative atomic ratio  $I^{\text{Cl}}/I^{\text{I}}$ , with  $\text{n} = \text{Cl}, \text{Pb}, \text{and N}$ , was investigated at the various p.e. takeoff angles; see Table 1.

**Table 1.** XPS Relative Atomic Ratio (multiplied by 100) as a Function of the p.e. Takeoff Angle

|                              | 10°            | 45°            | 70°            |
|------------------------------|----------------|----------------|----------------|
| $I^{\text{Pb}}/I^{\text{I}}$ | $42.2 \pm 0.5$ | $41.8 \pm 0.5$ | $43.3 \pm 0.5$ |
| $I^{\text{N}}/I^{\text{I}}$  | $18.0 \pm 0.5$ | $18.5 \pm 0.5$ | $17.5 \pm 0.5$ |
| $I^{\text{Cl}}/I^{\text{I}}$ | <0.6 (noise)   | $1.2 \pm 0.15$ | $2.1 \pm 0.1$  |

As can be noted from Table 1, differently from the cases of the  $I^{\text{N}}/I^{\text{I}}$  and  $I^{\text{Pb}}/I^{\text{I}}$ , which remain constant at the various investigated angles within the statistical uncertainty, the  $I^{\text{Cl}}/I^{\text{I}}$  atomic ratio significantly increases with the p.e. takeoff angle  $\theta$ . Figure 3 shows the  $I^{\text{Cl}}/I^{\text{I}}$  atomic ratio as a function of  $\sin(\theta)$ . The monotonic trend gives a clear and undoubted sign of a inhomogeneous distribution of the Cl atoms inside of the perovskite layer, with a major presence of the chloride species (Cl-rich region) at higher sampling depth, thus in proximity of the  $\text{TiO}_2$  surface. It is worth noting that a similar trend as a function of takeoff angle is observed also for the Cl/N atomic ratio. Because the nitrogen is independent of the presence of  $\text{PbI}_2$ , being, instead, strictly associated with the perovskite phase, this finding further reinforces our conclusion about the preferential location of chloride close to the perovskite/ $\text{TiO}_2$ . This important observation is, to our knowledge, unprece-

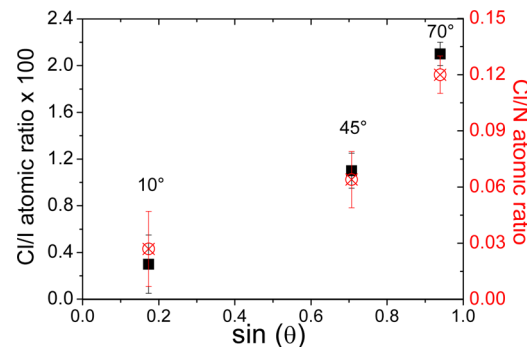


**Figure 3.** XPS  $I^{\text{Cl}}/I^{\text{I}}$  values multiplied by 100 (left axis) and  $I^{\text{Cl}}/I^{\text{N}}$  (right axis) as a function of  $\sin(\theta)$ , with  $\theta$  as the p.e. takeoff angle. A trend in the Cl content within the layer, while approaching the interface with the  $\text{TiO}_2$  substrate, is clearly stated.

dented in the current literature, and it basically constitutes the first evidence of the elusive presence of chloride in the  $\text{MAPbI}_{3-x}\text{Cl}_x$  mixed halide perovskite.

To investigate the energetics of chloride doping within the perovskite film and at the interface with  $\text{TiO}_2$ , along with assessing its possible effect on the interface electronic structure, we performed first-principles DFT simulations of the perovskite/ $\text{TiO}_2$  interface considering an extended model system; see Figure 4. We simulate here the (101)  $\text{TiO}_2$  anatase surface, which is the most abundant surface in  $\text{TiO}_2$  nanoparticles used for fabricating mesoporous  $\text{TiO}_2$  films. While we are aware that this could be not exactly representative of the surface of the flat  $\text{TiO}_2$  films employed for solar cell fabrication, we believe our results to be largely independent from the precise  $\text{TiO}_2$  topology, as discussed below. By considering the experimental lattice parameters of  $\text{TiO}_2$  ( $a = 18.92 \text{ \AA}$ ,  $b = 30.72 \text{ \AA}$ ), we build a  $3 \times 5 \times 3$  perovskite slab exposing the more stable (110) surfaces,<sup>27</sup> Figure 4. The chosen model was verified to introduce a lattice mismatch of only +0.36 and +1.92% along the  $\text{TiO}_2$   $a$  and  $b$  directions compared to the experimental lattice parameters of tetragonal  $\text{MAPbI}_3$  ( $a = b = 8.86$ ,  $c = 12.66$ ).<sup>29</sup> We then replaced 15 interfacial iodine atoms in  $\text{MAPbI}_3@\text{TiO}_2$  by chloride atoms to generate a  $\text{MAPbI}_{3-x}\text{Cl}_x@\text{TiO}_2$  interface model in which all chloride is positioned at the interface with  $\text{TiO}_2$  and considered also the possibility of 15 chlorine atoms being uniformly distributed in the perovskite film along the direction perpendicular to the  $\text{TiO}_2$  surface, Figure 4.

As previously noted, the interaction of the  $\text{MAPbI}_3$  perovskite with the  $\text{TiO}_2$  surface mainly takes place through binding of perovskite halide atoms to undercoordinated titanium atoms of the  $\text{TiO}_2$  surface.<sup>30</sup> When the interfacial iodine atoms are replaced by chloride, the interface topology is essentially unaltered, apart from a diminished distance between the two interacting fragments due to the shorter Cl–Ti bonds. Thus, considering the same type of interaction between  $\text{MAPbI}_3/\text{MAPbI}_{3-x}\text{Cl}_x$  perovskites and  $\text{TiO}_2$  and the fact that the majority of  $\text{TiO}_2$  surfaces all expose undercoordinated Ti atoms, it seems reasonable that our results would be independent from the precise  $\text{TiO}_2$  surface topology. Most notably, in line with the unfavorable energetics of chloride-to-iodide replacement in the bulk material previously predicted by some of us,<sup>31</sup> when displacing the chloride atoms away from the  $\text{TiO}_2$  surface, that is, when distributing them evenly in the perovskite slab, panel b in Figure 4, the total energy is found to rise by 0.7 eV compared to the all-surface chloride case, panel a

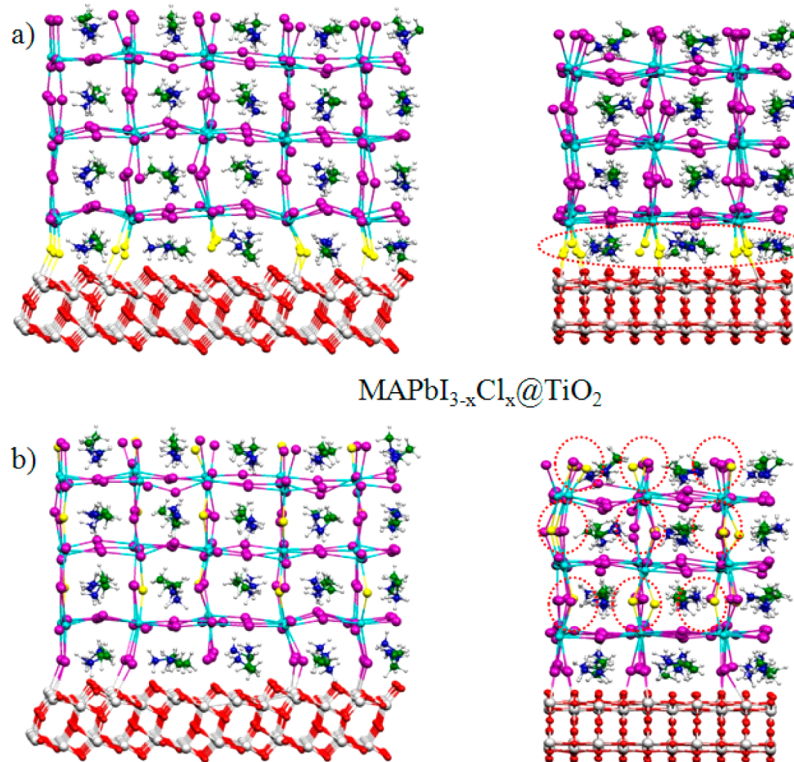


**Figure 4.** Optimized structures of (110)  $\text{MAPbI}_{3-x}\text{Cl}_x$  perovskite slabs interacting with the (101) anatase  $\text{TiO}_2$  surface. Notice the different location of chloride atoms (highlighted by red circles) in (a) (close to the  $\text{TiO}_2$  surface) and (b) (evenly distributed along the nonperiodic direction). Colors: Pb = light blue; I = magenta; Cl = yellow; Ti = light gray; O = red; C = green; N = blue; H = white.

in Figure 4. As a matter of fact, the  $\text{MAPbI}_{3-x}\text{Cl}_x$  perovskite BE to  $\text{TiO}_2$  decreases by 1.3 eV when chloride is displaced away from the  $\text{TiO}_2$  surface. These data clearly suggest that chloride will favorably interact with the  $\text{TiO}_2$  surface, rather than being dispersed into the perovskite film, in perfect agreement with the angular resolution in the Cl content inside of the layer revealed by XPS, also confirming previous joint theoretical and experimental results.<sup>26</sup>

The presence of chloride on the  $\text{TiO}_2$  surface could represent a key aspect for the proved superior charge-transport properties of the perovskite film and its structural order, besides partially explaining the difficulty of being detected in bulk through surface-sensitive techniques.<sup>10</sup> To gauge the electronic effect of interfacial chloride on the crucial perovskite/ $\text{TiO}_2$  interface, we report in Figure 5 an isodensity contour plot of the interface density of states (DOS) for the  $\text{MAPbI}_3$  and interfacial chloride  $\text{MAPbI}_{3-x}\text{Cl}_x$  perovskites interfaces with  $\text{TiO}_2$ , calculated including spin-orbit coupling (SOC).

This graph basically shows the joint system's integrated DOS as a function of energy ( $x$  axis) and of the distance from the  $\text{TiO}_2$  surface ( $y$  axis), identified by the dashed horizontal lines. The high DOS red/orange spots in the perovskite region in Figure 5 correspond to the I sp contributions to the valence band (VB), while the onset of the perovskite conduction band (CB, at  $\sim 0.8$  eV above the  $\text{TiO}_2$  CB, set at 0) is mainly contributed by Pb p states, partly hybridized with I p states.<sup>31</sup> In line with previous electronic structure analyses,<sup>31</sup> chloride contributes occupied states  $\sim 2$  eV below the top of the perovskite VB (see the red circles in Figure 5), while it has very little contribution to the perovskite CB bottom. Despite this indirect effect, the presence of interfacial chloride substantially alters the perovskite CB landscape, providing a strong

directional gradient of unoccupied states toward the  $\text{TiO}_2$  surface, as indicated by the arrow in Figure 5. While a small CB gradient is found also for the  $\text{MAPbI}_3$  case due to charge transfer to the  $\text{TiO}_2$  surface, such a gradient is strongly enhanced for the  $\text{MAPbI}_{3-x}\text{Cl}_x$  case, leading to a depletion (accumulation) of unoccupied states in the bulk (interface) region, as signaled by the arrow in Figure 5. This band bending toward the  $\text{TiO}_2$  surface leads, upon photoexcitation and creation of free carriers, to electrons being strongly funneled toward the  $\text{TiO}_2$  contact, while holes are delocalized across the perovskite film and partly pushed in the opposite direction, albeit with a smaller gradient. The picture extracted from our calculations seems consistent with the p-i-n representation of perovskite solar cells derived by Edri et al.,<sup>32</sup> and it also accounts for the observation again by Edri et al. of improved electron extraction in  $\text{MAPbI}_{3-x}\text{Cl}_x$  compared to  $\text{MAPbI}_3$  based solar cells.<sup>13</sup> The asymmetry in the VB/CB band bending would in turn strongly enhance the charge collection efficiency at the  $\text{TiO}_2$  electron-selective contact and possibly diminish the electron/hole recombination in the perovskite bulk and to some extent the recombination between electrons in the perovskite and holes in the hole-transporting material.

In conclusion, we have demonstrated by a combined experimental and theoretical approach the presence of chloride anions in mixed  $\text{MAPbI}_{3-x}\text{Cl}_x$  perovskite films and their preferential concentration at the interface with titanium dioxide.

Our achievement was accomplished by means of a high-sensitivity and nondestructive AR-XPS technique performed on extremely thin perovskite films deposited onto flat  $\text{TiO}_2$ . The variation of the p.e. takeoff angle allowed discriminating the chloride/iodide atomic ratio through the layer, permitting an

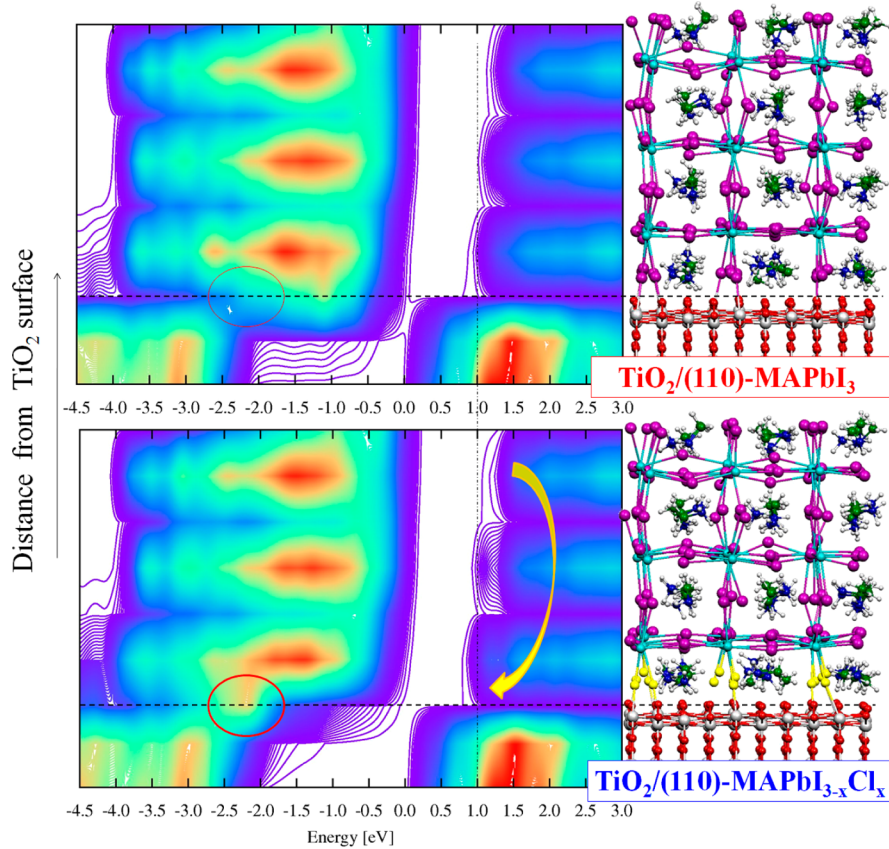


**Figure 5.** Isodensity plot of the integrated DOS as a function of the distance from the  $\text{TiO}_2$  surface for  $\text{MAPbI}_3$  and interfacial chloride  $\text{MAPbI}_{3-x}\text{Cl}_x$  perovskite interfaces with  $\text{TiO}_2$ . A blue to red color variation indicates an increase of the DOS value. The red circles highlight in both cases the energy range where occupied chloride states are found in  $\text{MAPbI}_{3-x}\text{Cl}_x$  (and are lacking in  $\text{MAPbI}_3$ ). The arrow in the lower panel indicates the sizable band bending observed in the  $\text{MAPbI}_{3-x}\text{Cl}_x$  case.

elective investigation at the perovskite/ $\text{TiO}_2$  heterointerface. DFT calculations confirm a favorable chloride– $\text{TiO}_2$  interaction  $n$ , which could explain the XPS results. Most notably, our calculations indicate a chloride-induced bending of the perovskite CB at the interface with titania, which could in turn facilitate the electron extraction/collection efficiency of the solar cell. Such a behavior, which is clearly not present in the case of the pure  $\text{MAPbI}_3$  perovskite, has important implications on the perovskite/electron transporting layer interface energetics, providing a pathway for improved electron collection efficiency. Intentional and controlled doping with chloride or other species could represent a novel opportunity to modify the hybrid perovskite materials and improve the device performance. Our finding can be definitely considered as a platform/launching pad for further studies on the role of chloride in  $\text{MAPbI}_{3-x}\text{Cl}_x$ .

## ■ EXPERIMENTAL METHODS

**Material Preparation.** Methylamine ( $\text{CH}_3\text{NH}_2$ ) solution, 33 wt % in absolute ethanol, was reacted with hydroiodic acid (HI), 57 wt % in water, with excess methylamine under a nitrogen atmosphere in ethanol at room temperature. Typical quantities were 24 mL of methylamine, 10 mL of HI, and 100 mL of ethanol. Crystallization of methylammonium iodide (MAI) was achieved using a rotary evaporator; a white-colored powder was formed, indicating successful crystallization. Methylammonium MAI and lead(II) chloride ( $\text{PbCl}_2$ ) were dissolved in anhydrous *N,N*-dimethylformamide (DMF) at a 3:1 molar ratio, to

produce a  $\text{MAPbI}_{3-x}\text{Cl}_x$  precursor solution. MAI and lead (II) iodide ( $\text{PbI}_2$ ) were dissolved in anhydrous DMF in a 1:1 molar ratio to produce a  $\text{MAPbI}_3$  precursor solution.

**Device Fabrication and Characterization.** FTO glasses (Pilkington, TEC15, 15 Ohm/sq) were etched with metallic Zn and HCl (2 M) and washed with water and cleaned in an ultrasonic bath in acetone and isopropanol for 10 min each. Then, they were immersed into a TL1 washing solution ( $\text{H}_2\text{O}_2/\text{NH}_3/\text{H}_2\text{O}$  5:1:1, v/v) and heated to 80 °C for 10 min to remove organic contamination. To make a compact  $\text{TiO}_2$  blocking layer of ~60 nm, the cleaned FTO glasses were coated with 0.15 M titanium diisopropoxide bis(acetylacetone) (75% Aldrich) in 1-butanol (Aldrich) solution by the spin-coating (2000 rpm), which was heated at 125 °C for 5 min. After the coated film was cooled down to room temperature, the same process was repeated twice with 0.3 M titanium diisopropoxide bis(acetylacetone) solution in 1-butanol. The coated FTO glasses with  $\text{TiO}_2$  precursor solutions were heated at 450 °C for 15 min.

The 20 wt %  $\text{MAPbI}_3$  perovskite precursor solution was spin-coated onto the compact  $\text{TiO}_2$  layer film at 3000 rpm for 45 s in  $\text{N}_2$  atmosphere and annealed on a hot plate at 100 °C for 15 min. The 20 wt %  $\text{MAPbI}_{3-x}\text{Cl}_x$  was deposited on a preheated (100 °C)  $\text{TiO}_2$  substrate at 2000 rpm for 45 s, followed by annealing at 100 °C for 1 h.

A chlorobenzene solution containing 131 mM spiro-OMeTAD, 216 mM *tert*-butylpyridine, and 58 mM lithium bis(trifluoromethylsilyl)imide salt was cast onto the perov-

skite-coated substrate and spun at a rate of 2500 rpm for 45 s. Cells were completed by thermal evaporation of 200 nm Ag electrodes and exposed to air for 3 h before characterization. The active area was  $0.09\text{ cm}^2$  for all the devices, which were characterized under an Air Mass 1.5 Global (AM 1.5 G) solar simulator with an irradiation intensity of  $100\text{ mW}\cdot\text{cm}^{-2}$ .

## ■ COMPUTATIONAL DETAILS

Geometry optimizations were carried out at the PBE-GGA<sup>33</sup> level with the SIESTA 3.0 program package<sup>34</sup> using a DZ basis set along with PBE scalar-relativistic pseudopotential for Ti, I, Cl, O, C, N, and H atoms. Pb atoms were treated with the WC-GGA<sup>35</sup> scalar-relativistic pseudopotential. Electrons from I 5s,5p; Cl 3s,3p; O, N, and C 2s,2p; H 1s; Ti 4s,3d; Pb 6s,6p,5d shells were explicitly included in the calculations. A value of 100 Ry was used as the plane wave cutoff for the grid. Spin-orbit interactions were not included in SIESTA calculations.

Our model system was made of a  $3 \times 5 \times 3$  pseudocubic perovskite slab exposing the 110 surfaces. The perovskite slab stoichiometry was  $\text{MA}_{60}\text{Pb}_{45}\text{I}_{150}$  ( $\text{MA}_{60}\text{Pb}_{45}\text{I}_{135}\text{Cl}_{15}$  for the chlorine-doped materials), and thus, it deviated from the ideal material stoichiometry, in line with the analysis of perovskites surfaces by Mitzi.<sup>36</sup> By following the same approach as that reported in our previous work,<sup>30</sup> we “deposited” the  $3 \times 5 \times 3$  pseudocubic perovskite slab, exposing the 110 surfaces onto a  $5 \times 3 \times 2$   $\text{TiO}_2$  slab. As already reported,<sup>30</sup> the interaction of the  $\text{MAPbI}_3$  perovskite with the  $\text{TiO}_2$  surface mainly took place through binding of undercoordinated perovskite iodide atoms to undercoordinated titanium atoms of the  $\text{TiO}_2$  surface.<sup>30</sup> The experimental  $\text{TiO}_2$  cell parameters ( $a = 18.92\text{ \AA}$ ,  $b = 30.72\text{ \AA}$ ) were employed to build a periodic supercell in the  $x$  and  $y$  directions, leaving  $10\text{ \AA}$  vacuum along the  $z$  direction.

Electronic structure analyses were performed with the Quantum Espresso program package<sup>37</sup> on the structures optimized by SIESTA. Electron–ion interactions were described by ultrasoft pseudopotentials with electrons from O, N, and C 2s,2p; H 1s; Ti 3s,3p,3d,4s; Pb 6s,6p,5d; I 5s,5p; Cl 3s,3p shells explicitly included in the calculations. Plane wave basis set cutoffs for the smooth part of the wave functions and the augmented density were 25 and 200 Ry, respectively. Electronic structure calculations were performed including SOC. We previously checked that SIESTA and Quantum Espresso provide perfectly coherent results for the  $\text{MAPbI}_3$  perovskite slab and for its interface with  $\text{TiO}_2$ .<sup>30</sup>

**X-ray Photoelectron Spectroscopy (XPS) Details.** XPS analyses were performed by using a PHI ESCA/SAM 5600 Multy technique spectrometer equipped with a Mg K $\alpha$  X-ray source at a pressure of  $5 \times 10^{-9}$  Torr. Measurements were performed at different electron takeoff angles (angles between the surface of the sample and the detector), namely, 10, 45, and 70°, with an angular acceptance of  $\pm 5^\circ$ . The BE scale was calibrated by centring the C 1s signal due to the adventitious/hydrocarbon carbon at 285.0 eV.

## ■ ASSOCIATED CONTENT

### S Supporting Information

Absorption spectra, X-ray diffraction, X-ray reflectivity, atomic force microscopy, and XPS survey of the  $\text{MAPbI}_{3-x}\text{Cl}_x/\text{TiO}_2$  bilayer. This material is available free of charge via the Internet at <http://pubs.acs.org>.

## ■ AUTHOR INFORMATION

### Corresponding Authors

- \*E-mail: silvia.coletta@nano.cnr.it (S.C.).
- \*E-mail: filippo@thch.unipg.it (F.D.A.).
- \*E-mail: giovanna.pellegrino@imm.cnr.it (G.P.).

### Notes

The authors declare no competing financial interest.

## ■ ACKNOWLEDGMENTS

This work was supported by Progetto di ricerca PON R&C 2007-2013 (Avviso n. 713/Ric. del 29 ottobre 2010) MAAT-Molecular NAnotechnology for HeAlth and EnvironmenT (Project Number: PON02\_00563\_3316357), EFOR-Energia da FOnti Rinnovabili (Iniziativa CNR per il Mezzogiorno L. 191/2009 art. 2 comma 44), PHOEBUS-reti laboratori regione Puglia and Daunia Wind. S.C. and G.G. gratefully acknowledge the project PON BEYON-NANO (Materials and processes BEYOND the NANO-scale). The authors gratefully acknowledge Emanuele Smecca for useful discussions.

## ■ REFERENCES

- (1) Zhou, H.; Chen, Q.; Li, G.; Luo, S.; Song, T.; Duan, H.-S.; Hong, Z.; You, J.; Liu, Y.; Yang, Y. Interface Engineering of Highly Efficient Perovskite Solar Cells. *Science* **2014**, *345*, 542.
- (2) Snaith, H. J. Perovskites: The Emergence of a New Era for Low-Cost, High-Efficiency Solar Cells. *J. Phys. Chem. Lett.* **2013**, *4*, 3623–3630.
- (3) Laban, A. W.; Etgar, L. Depleted Hole Conductor-Free Lead Halide Iodide Heterojunction Solar Cells. *Energy Environ. Sci.* **2013**, *6*, 3249–3253.
- (4) Burschka, J.; Pellet, N.; Moon, S. J.; Humphry-Baker, R.; Gao, P.; Nazeeruddin, M. K.; Gratzel, M. Sequential Deposition As a Route to High-Performance Perovskite-Sensitized Solar Cells. *Nature* **2013**, *499*, 316–319.
- (5) Chung, I.; Lee, B.; He, J. Q.; Chang, R. P. H.; Kanatzidis, M. G. All-Solid-State Dye-Sensitized Solar Cells with High Efficiency. *Nature* **2012**, *485*, 486–494.
- (6) Liu, M. Z.; Johnston, M. B.; Snaith, H. J. Efficient Planar Heterojunction Perovskite Solar Cells by Vapour Deposition. *Nature* **2013**, *501*, 395.
- (7) Suarez, B.; Gonzalez-Pedro, V.; Ripolles, T. S.; Sanchez, R. S.; Otero, L.; Mora-Sero, I. Recombination Study of Combined Halides (Cl, Br, I) Perovskite Solar Cells. *J. Phys. Chem. Lett.* **2014**, *1628–1635*.
- (8) Wehrenfennig, C.; Eperon, G. E.; Johnston, M. B.; Snaith, H. J.; Herz, L. M. High Charge Carrier Mobilities and Lifetimes in Organolead Trihalide Perovskites. *Adv. Mater.* **2014**, *26*, 1584–1589.
- (9) Lee, M. M.; Teuscher, J.; Miyasaka, T.; Murakami, T. N.; Snaith, H. J. Efficient Hybrid Solar Cells Based on Meso-Superstructured Organometal Halide Perovskites. *Science* **2012**, *338*, 643–647.
- (10) Docampo, P.; Hanusch, F.; Stranks, S. D.; Döblinger, M.; Feckl, J. M.; Ehrenspurger, M.; Minar, N. K.; Johnston, M. B.; Snaith, H. J.; Bein, T. Solution Deposition-Conversion for Planar Heterojunction Mixed Halide Perovskite Solar Cells. *Adv. Energy Mater.* **2014**, DOI: 10.1002/aenm.201400355.
- (11) Zhao, Y.; Zhu, K.  $\text{CH}_3\text{NH}_3\text{Cl}$ -Assisted One-Step Solution Growth of  $\text{CH}_3\text{NH}_3\text{PbI}_3$ : Structure, Charge-Carrier Dynamics, and Photovoltaic Properties of Perovskite Solar Cells. *J. Phys. Chem. C* **2014**, *118*, 9412–9418.
- (12) Edri, E.; Kirmaier, S.; Henning, A.; Mukhopadhyay, S.; Gartsman, K.; Rosenwaks, Y.; Hodes, G.; Cahen, D. Why Lead Methylammonium Tri-Iodide Perovskite-Based Solar Cells Require a Mesoporous Electron Transporting Scaffold (But Not Necessarily a Hole Conductor). *Nano Lett.* **2014**, *14*, 1000–1004.
- (13) Edri, E.; Kirmaier, S.; Kulbak, M.; Hodes, G.; Cahen, D. Chloride Inclusion and Hole Transport Material Doping to Improve

- Methyl Ammonium Lead Bromide Perovskite-Based High Open-Circuit Voltage Solar Cells. *J. Phys. Chem. Lett.* **2014**, *5*, 429–433.
- (14) Stranks, S. D.; Eperon, G. E.; Grancini, G.; Menelaou, C.; Alcocer, M. J. P.; Leijtens, T.; Herz, L. M.; Petrozza, A.; Snaith, H. J. Electron–Hole Diffusion Lengths Exceeding 1 Micrometer in an Organometal Trihalide Perovskite Absorber. *Science* **2013**, *342*, 341–344.
- (15) Conings, B.; Baeten, L.; De Dobbelaere, C.; D’Haen, J.; Manca, J.; Boyen, H.-G. Perovskite-Based Hybrid Solar Cells Exceeding 10% Efficiency with High Reproducibility Using a Thin Film Sandwich Approach. *Adv. Mater.* **2014**, *26*, 2041–2046.
- (16) Pellegrino, G.; Alberti, A.; Condorelli, G. G.; Giannazzo, F.; Magna, A. L.; Paoletti, A. M.; Pennesi, G.; Rossi, G.; Zanotti, G. Study of the Anchoring Process of Tethered Unsymmetrical Zn-Phthalocyanines on TiO<sub>2</sub> Nanostructured Thin Films. *J. Phys. Chem. C* **2013**, *117*, 11176–11185.
- (17) Alberti, A.; Pellegrino, G.; Condorelli, G. G.; Bongiorno, C.; Morita, S.; La Magna, A.; Miyasaka, T. Efficiency Enhancement in ZnO:Al-Based Dye-Sensitized Solar Cells Structured with Sputtered TiO<sub>2</sub> Blocking Layers. *J. Phys. Chem. C* **2014**, *118*, 6576–6585.
- (18) Alberti, A.; De Marco, L.; Pellegrino, G.; Condorelli, G. G.; Giannuzzi, R.; Scarfiello, R.; Manca, M.; Spinella, C.; Gigliand, G.; La Magna, A. A Combined Strategy to Realize Efficient Photoelectrodes for Low Temperature Fabrication of Dye Solar Cells. *ACS Appl. Mater. Interfaces* **2014**, *6*, 6425–6433.
- (19) Alberti, A.; Buongiorno, C.; Pellegrino, G. Anatse/Rutile Nucleation and Growth on (0002) And (11–20) Oriented ZnO:Al/Glass Substrates at 150°C. *Thin Solid Films* **2014**, *555*, 3–8.
- (20) Saliba, M.; Tan, K. W.; Sai, H.; Moore, D. T.; Scott, T.; Zhang, W.; Estroff, L. A.; Wiesner, U.; Snaith, H. J. The Influence of Thermal Processing Protocol upon the Crystallization and Photovoltaic Performance of Organic–Inorganic Lead Trihalide Perovskites. *J. Phys. Chem. C* **2014**, *118*, 17171–17177.
- (21) Eperon, G. E.; Burlakov, V. M.; Docampo, P.; Goriely, A.; Snaith, H. J. Morphological Control for High Performance, Solution-Processed Planar Heterojunction Perovskite Solar Cells. *Adv. Funct. Mater.* **2014**, *24*, 151–157.
- (22) Gonzalez-Pedro, V.; Juárez-Pérez, E. J.; Arsyad, W. S.; Barea, E. M.; Fabregat-Santiago, F.; Mora-Sero, I.; Bisquert, J. General Working Principles of CH<sub>3</sub>NH<sub>3</sub>PbX<sub>3</sub> Perovskite Solar Cells. *Nano Lett.* **2014**, *14*, 888–893.
- (23) Liu, D.; Kelly, T. L. Perovskite Solar Cells with a Planar Heterojunction Structure Prepared Using Room-Temperature Solution Processing Techniques. *Nat. Photonics* **2014**, *8*, 133.
- (24) Jeon, N. J.; Lee, H. G.; Kim, Y. C.; Seo, J.; Noh, J. H.; Lee, J.; Seok, S. I. o-Methoxy Substituents in Spiro-OMeTAD for Efficient Inorganic–Organic Hybrid Perovskite Solar Cells. *J. Am. Chem. Soc.* **2014**, *136*, 7837–7840.
- (25) Li, H.; Fu, K.; Hagfeldt, A.; Graetzel, M.; Mhaisalkar, S. G.; Grimsdale, A. C. A Simple 3,4-Ethylenedioxythiophene Based Hole-Transporting Material for Perovskite Solar Cells. *Angew. Chem., Int. Ed.* **2014**, *53*, 4085–4088.
- (26) Colella, S.; Mosconi, E.; Fedeli, P.; Listorti, A.; Gazza, F.; Orlandi, F.; Ferro, P.; Besagni, T.; Rizzo, A.; Calestani, et al. MAPbI<sub>(3-x)</sub>Cl<sub>x</sub> Mixed Halide Perovskite for Hybrid Solar Cells: The Role of Chloride as Dopant on the Transport and Structural Properties. *Chem. Mater.* **2013**, *25*, 4613–4618.
- (27) Mosconi, E.; De Angelis, F. First Principles Investigation of the TiO<sub>2</sub>/Organohalide Perovskites Interface: The Role of Interfacial Chlorine. *J. Phys. Chem. Lett.* **2014**, *5*, 2619–2625.
- (28) Kishi, K.; Ikeda, S. X-ray Photoelectron Spectroscopic Study of the Reaction of Evaporated Metal Films with Chlorine Gas. *J. Phys. Chem.* **1974**, *78*, 107–112.
- (29) Poglitsch, A.; Weber, D. Dynamic Disorder in Methylammoniumtrihalogenoplumbates (II) Observed by Millimeter-Wave Spectroscopy. *J. Chem. Phys.* **1987**, *87*, 6373–6378.
- (30) Roiati, V.; Mosconi, E.; Listorti, A.; Colella, S.; Gigli, G.; De Angelis, F. Stark Effect in Perovskite/TiO<sub>2</sub> Solar Cells: Evidence of Local Interfacial Order. *Nano Lett.* **2014**, *14*, 2168–2174.
- (31) Mosconi, E.; Amat, A.; Nazeeruddin, M. K.; Grätzel, M.; De Angelis, F. First-Principles Modeling of Mixed Halide Organometal Perovskites for Photovoltaic Applications. *J. Phys. Chem. C* **2013**, *117*, 13902–13913.
- (32) Edri, E.; Mukhopadhyay, S. K. S.; Gartsman, K.; Hodes, G.; Cahen, D. Elucidating the Charge Carrier Separation and Working Mechanism of CH<sub>3</sub>NH<sub>3</sub>PbI<sub>3-x</sub>Cl<sub>x</sub> Perovskite Solar Cells. *Nat. Commun.* **2014**, *5*, 3461.
- (33) Perdew, J. P.; Burke, K.; Ernzerhof, M. Generalized Gradient Approximation Made Simple. *Phys. Rev. Lett.* **1996**, *77*, 3865–3868.
- (34) José, M. S.; Emilio, A.; Julian, D. G.; Alberto, G.; Javier, J.; Pablo, O.; Daniel, S.-P. The SIESTA Method for Ab Initio Order-N Materials Simulation. *J. Phys.: Condens. Matter* **2002**, *14*, 2745.
- (35) Wu, Z.; Cohen, R. E. More Accurate Generalized Gradient Approximation for Solids. *Phys. Rev. B* **2006**, *73*, 235116.
- (36) Mitzi, D. B. Solution-Processed Inorganic Semiconductors. *J. Mater. Chem.* **2004**, *14*, 2355–2365.
- (37) Giannozzi, P.; Baroni, S.; Bonini, N.; Calandra, M.; Car, R.; Cavazzoni, C.; Ceresoli, D.; Chiarotti, G. L.; Cococcioni, M.; Dabo, I.; et al. QUANTUM ESPRESSO: A Modular and Open-Source Software Project for Quantum Simulations of Materials. *J. Phys.: Condens. Matter* **2009**, *21*, 395502.